Chemical Geology 644 (2024) 121843

Contents lists available at ScienceDirect

Chemical Geology

journal homepage: www.elsevier.com/locate/chemgeo

Extreme Sn isotope fractionation in highly evolved granites

Ke-Ke Sun [a], Jia-Xin She [b], De-Hong Du [b], Weiqiang Li [b,*], Jun Deng [c,*]

[a] School of Earth Sciences and Engineering, Hohai University, Nanjing, Jiangsu 211100, PR China
[b] State Key Laboratory for Mineral Deposits Research, School of Earth Sciences and Engineering, Nanjing University, Nanjing, Jiangsu 210023, PR China
[c] State Key Laboratory of Geological Processes and Mineral Resources, China University of Geosciences, Beijing 100083, PR China

ARTICLE INFO

Editor: Claudia Romano

Keywords:
Sn isotope fractionation
Highly evolved granite
Fractional crystallization
Fluid exsolution
Gejiu

ABSTRACT

Stable Sn isotopes have been widely used to trace the planetary differentiation processes, the provenance and trade paths of ancient bronze artifacts, the mineralization history of tin ore deposits, and the terrestrial magmatic processes. However, systematic Sn isotope studies of felsic igneous rocks especially the Sn mineralization-related highly evolved granites are still lacking. In this study, we present the first high-precision Sn isotope data of two Sn-rich highly evolved S-type granites (Laochang and Kafang) from the world-class Gejiu Sn ore district. These granite samples show remarkably variable $\delta^{122/118}$Sn values (relative to the Sn standard solution NIST 3161a) ranging from 0.11 ± 0.02‰ to 0.93 ± 0.02‰ (2σ), which is the largest variation range reported in granites so far. The absence of correlations between Sn isotopes and LOI (loss-on-ignition) and $\varepsilon_{Nd}(t)$ values, along with the low magmatic oxygen fugacity ($\triangle$FMQ < 0) for these granites, rule out hydrothermal alteration, wall-rock assimilation, source composition heterogeneity, and anatexis processes as causes of the Sn isotope fractionation. The Laochang granites show negative correlations between $\delta^{122/118}$Sn values and magmatic differentiation indicators (e.g., CaO, Fe_2O_3, Ti, Eu/Eu*, F/Cl), suggesting fractional crystallization increased the $\delta^{122/118}$Sn isotopes in the residual melts. The fractional crystallized minerals are mainly composed of biotite, plagioclase, and minor ilmenite. Compared with the Laochang granites, the Kafang granites show higher SiO_2 contents, F/Cl ratios, and $\delta^{122/118}$Sn values, suggesting the magma at this stage was fluid-saturated and fluid exsolution coupled with fractional crystallization would further enrich the heavy Sn isotopes in the residual melts. We further quantified the contributions of crystal fractionation and fluid exsolution on Sn isotopic variability using a Rayleigh fractionation model. The modeling indicates that $\triangle^{122/118}Sn_{crystal\text{-}melt} = -0.6$ to −0.5‰ and $\triangle^{122/118}Sn_{fluid\text{-}melt} = -1.9$ to −0.7‰ with an initial H_2O content of 2 wt.% can explain the observed $\delta^{122/118}$Sn values of Gejiu granites. This study implies that both crystal fractionation and fluid exsolution processes cause increase of Sn isotopic values in the highly evolved granites and Sn isotopes are useful for tracing the evolution of highly differentiated igneous rocks.

1. Introduction

Tin is an element of complex and interesting properties, acting as volatile, chalcophile, siderophile, and moderately incompatible element during geological and cosmochemical processes. Tin has ten stable isotopes with atomic mass ranging from 112 to 124, and Sn isotopic variations have been identified in igneous rocks, tin ores, bronze artifacts, and experiments (Badullovich et al., 2017; Brügmann et al., 2017; Creech et al., 2017; Liu et al., 2021; She et al., 2020; Wang et al., 2019; Wang et al., 2018; Wang et al., 2017; Yamazaki et al., 2013; Yao et al., 2018; Zhang et al., 2023; Zhou et al., 2022). Sn isotopes of cassiterite (SnO_2) can be used to trace the magmatic-hydrothermal mineralization processes of tin ore deposits (Liu et al., 2021; Yao et al., 2018; Zhou et al., 2022; Wu et al., 2023), the provenance and trade paths of ancient bronze artifacts (Haustein et al., 2010; Yamazaki et al., 2013; Yamazaki et al., 2014). Experiments confirm both redox reactions and evaporation of Sn-bearing solutions are valid mechanisms induce Sn isotope fractionation (She et al., 2020; Wang et al., 2019). Significant Sn isotope fractionation during mantle partial melting and differentiation has also been reported (Badullovich et al., 2017; Wang et al., 2018). During partial melting of peridotite, Sn^{4+} with an isotopically heavier composition exhibits greater incompatibility than Sn^{2+} and is enriched in the silicate melt relative to the residue, resulting in isotopically lighter peridotite and isotopically heavier basaltic melts (Wang et al., 2018).

* Corresponding authors.
E-mail addresses: liweiqiang@nju.edu.cn (W. Li), djun@cugb.edu.cn (J. Deng).

https://doi.org/10.1016/j.chemgeo.2023.121843
Received 24 August 2023; Received in revised form 14 November 2023; Accepted 18 November 2023
Available online 23 November 2023

Crystal fractionation of ilmenite would result in residual magma being enriched in light Sn isotopes during basaltic magma differentiation (Badullovich et al., 2017). To date, except for reported data for several geological reference materials, systematic Sn isotope studies of intermediate and felsic igneous rocks are still limited (Creech et al., 2017; Wang et al., 2017; Wang et al., 2022; She et al., 2023b).

Primary Sn mineralization is generally associated with highly differentiated and relatively reduced granitic magmas (Ishihara, 1977; Lehmann, 1982, 2021; Lehmann and Mahawat, 1989). Sn-rich granites commonly experience complex evolution processes including extended fractional crystallization and late-stage fluid exsolution (Harlaux et al., 2021; Lehmann, 2021). Sn is incompatible during the crystallization of granitic magma and is fluid-mobile that can migrate with magmatic hydrothermal fluids. Therefore, Sn-rich highly evolved granites should be an ideal object for investigating Sn isotopes behavior during magmatic-hydrothermal evolution process. However, there have been no systematic studies on the Sn isotope compositions of highly differentiated granites. This hampers the application of Sn isotopes to trace the granite genesis and subsequent magmatic-hydrothermal processes.

The Gejiu Sn polymetallic ore deposit, located at the western margin of the Cathaysia block, South China, is one of the largest Sn deposits in the world (Cheng et al., 2013b; Sun et al., 2023). Tin mineralization in

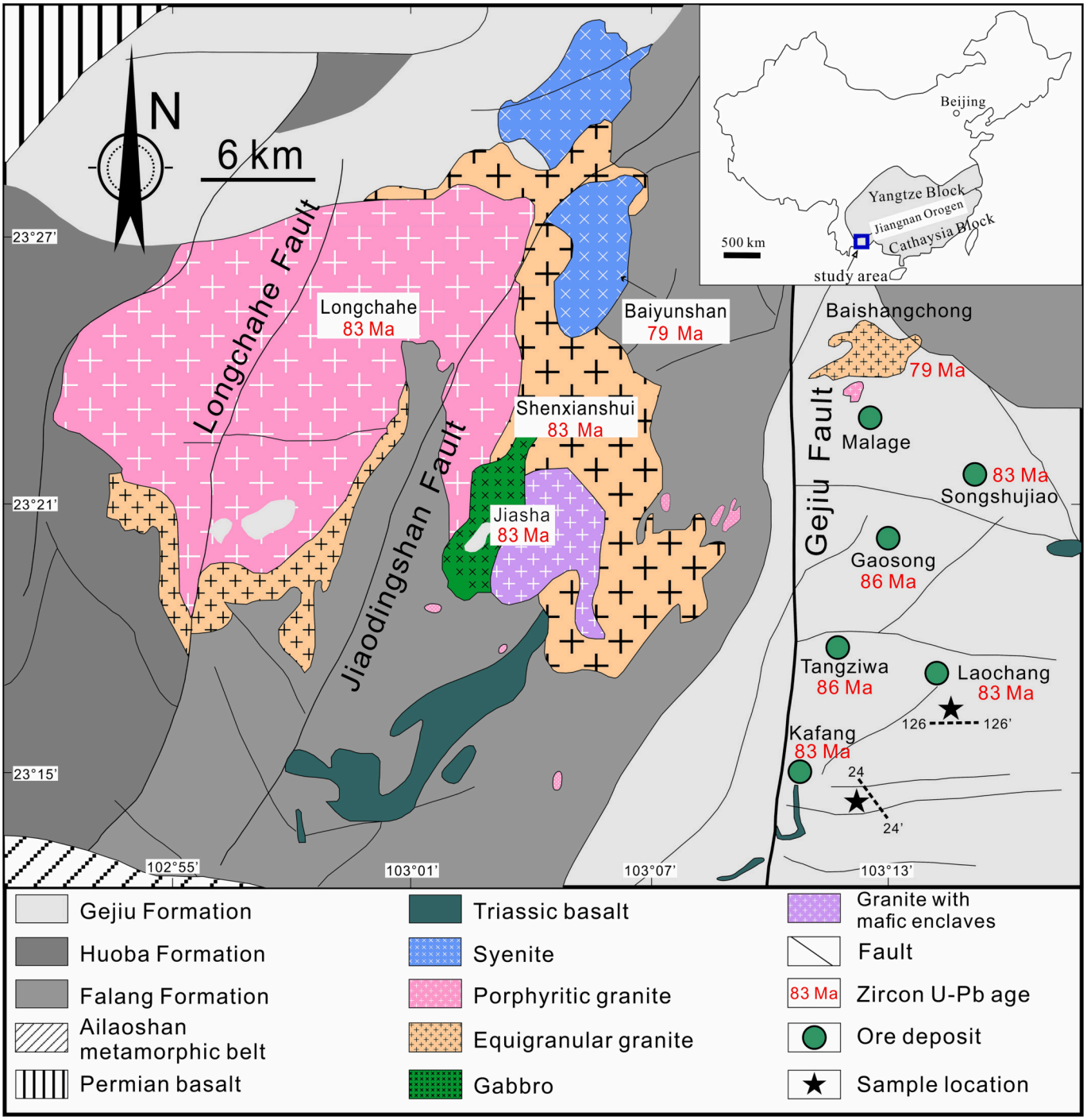

Fig. 1. Geological map of the Gejiu district, showing the distribution of Late Cretaceous intrusions and tin-polymetallic deposits. Zircon U—Pb ages are from Cheng and Mao (2010).

the Gejiu district is related to highly evolved S-type granites (Xu et al., 2021; Sun et al., 2023). The source composition and evolutionary history of the Gejiu Sn-rich granites have been well established, offering an excellent opportunity to explore the behavior of Sn isotopes during magmatic evolution of granitic magmas. In this study, we present whole-rock Sn isotopic and halogen (F, Cl) content data from a suite of well-characterized Sn-rich high-SiO_2 granites from the Gejiu district, in order to constrain the Sn isotope behavior in magmatic-hydrothermal systems. Our results reveal ~1 per mil (‰) Sn isotope variation in the Gejiu granite samples, revealing key Sn-mineralization controlling processes of biotite and plagioclase fractionation, and subsequent magmatic-hydrothermal fluid exsolution.

2. Geological setting and samples

The South China block consists of the Yangtze block in the northwest, the Cathaysia block in the southeast, and the Jiangnan orogenic belt in between (Fig. 1). South China is one of the most important metallogenic provinces in the world and is well known for its Mesozoic granitic magmatism and W–Sn mineralization events (Mao et al., 2013). A series of world-class Sn polymetallic deposits including Gejiu, Dachang, and Dulong deposits are distributed along the western margin of the South China block (Fig. 1). The Gejiu Sn polymetallic ore district, located about 300 km southeast of Kunming, Yunnan Province, is the largest primary tin deposit in the world. The dominant strata in the Gejiu district are the Middle Triassic Gejiu and Falang Formations and Upper Triassic Huoba Formation. Minor Proterozoic Ailaoshan metamorphic rocks and Triassic basalts are also exposed in the district (Fig. 1). The Gejiu Formation is the main ore-host strata that consists of 400–1400 m thick limestone and minor intercalated dolomitic limestone, dolostone, and mafic lavas. The Falang Formation consists of approximately 3000 m thick sequence of sandstone and limestone with minor mafic lavas, which overlie the Gejiu Formation. The Huoba Formation is mainly composed of 500–1200 m thick shale, sandstone, and siltstone. The Ailaoshan metamorphic zone, located on the southwestern margin of the Gejiu district, is mainly composed of sillmanite-bearing gneisses. The dominant structures in the Gejiu district are three sets of faults striking NS, NNE, and NW, respectively (Fig. 1). The N-S trending Gejiu fault is the dominant structure in the study area, separating the Gejiu area into eastern and western sectors. The Sn deposits are mainly distributed in the eastern sector. A suite of *E*-W trending secondary faults control the locations of the granites and ore deposits, separating the Gejiu district into Malage, Songshujiao, Gaosong, Tangziwa, Laochang, and Kafang ore deposits from North to South (Cheng et al., 2013a; Xu et al., 2021; Sun et al., 2023). Late Cretaceous intrusions are well developed in the Gejiu district and mainly consist of gabbro, mafic microgranular enclave-bearing monzogranite, porphyritic biotite granite, equigranular granite, syenite and minor mafic dikes. Mafic-intermediate and alkaline rocks are mainly distributed in the western sector and granites occur throughout the region (Fig. 1). These igneous rocks intruded into the Gejiu and Falang Formations and crystallized at 79–86 Ma, which are well exposed in the western sector but mainly concealed at a depth of 200 to 1000 m below the surface in the eastern sector (Cheng and Mao, 2010). Tin mineralization is associated with the porphyritic and equigranular granites in the eastern sector of the Gejiu district.

Eight equigranular granite samples collected from the Zhuyeshan tunnel (at elevation 1560 m above sea level) in the Laochang ore deposit and seven samples from the Qianjin tunnel (at elevation 1800 m above sea level) in the Kafang ore deposit were used for Sn isotopic analysis in this study (Fig. 2; Xu et al., 2022b; Sun et al., 2023). Both the Laochang and the Kafang granites show fine-grained granular textures with a mineral assemblage of quartz, plagioclase, K-feldspar, biotite, muscovite, and accessory minerals including zircon, ilmenite, apatite, and fluorite (Fig. 3). The Laochang granite is composed of 30% quartz, 30% plagioclase, 25% K-feldspar, 10–15% biotite, and 2% accessory minerals. Hydrothermal alteration consists of minor replacement of

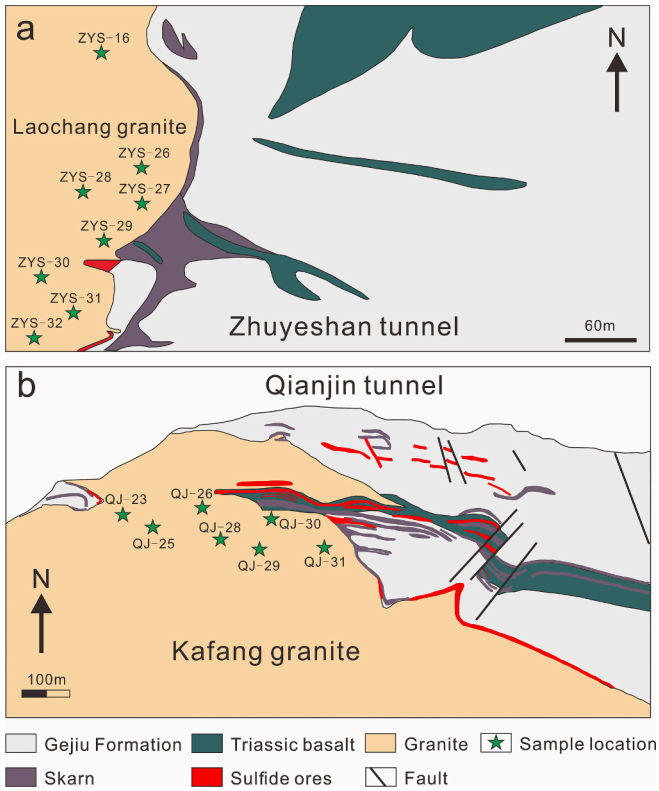

Fig. 2. Geological map of the Laochang and Kafang deposits, showing the main rock types, structures, and samples location. (a) Geological cross section map of the Zhuyeshan tunnel (at elevation 1560 m above sea level) from Laochang deposit (Yunnan Tin Group, pers. Commun., 2023); (b) geological cross section map of the Qianjin tunnel (at elevation 1800 m above sea level) from Kafang deposit (modified from Sun et al., 2023).

plagioclase and biotite by sericite and muscovite, altogether represent ~5% of the rock volume (Fig. 3). The Kafang granite comprises 30% quartz, 40–45% K-feldspar, 10–15% plagioclase, 5–10% biotite, and 5–10% muscovite. Minor K-feldspar and biotite were altered to kaolinite and chlorite, representing ~8% of the rock volume (Fig. 3). The Laochang granite has a higher proportion of biotite than the Kafang granite. The Laochang granites are metaluminous to peraluminous and have high contents of SiO_2 (71.2–75.1 wt%), alkalines ($K_2O + Na_2O$ = 7.21–8.48 wt%), and low contents of Fe_2O_3 (1.46–2.80 wt%), MgO (0.30–0.59 wt%), TiO_2 (0.14–0.30 wt%), and CaO (0.79–1.65 wt%) (Fig. 4). In the chondrite-normalized REE patterns, these samples have light rare earth element-enriched patterns with negative Eu anomalies ($(La/Yb)_N$ = 10.6–19.0; Eu/Eu* = 0.16–0.26; Fig. 5a). In upper continental crust-normalized diagrams, they are enriched in Li, Rb, Y, Nb, Sn, Cs, Ta, Pb, Th, and U and depleted in Sc, V, Cr, Co, Ni, Sr, and Ba (Fig. 5b). They have low whole-rock ε_{Nd} values (−9.0 to −8.3), zircon ε_{Hf} values (−8.2 to −5.9), and high zircon $\delta^{18}O$ values (7.3–8.9‰) (Xu et al., 2022b). The Kafang granite samples are also metaluminous to peraluminous and have higher contents of SiO_2 (74.03–78.24 wt%), alkaline ($K_2O + Na_2O$ = 6.93–8.93 wt%), and lower contents of Fe_2O_3 (0.08–1.40 wt%), MgO (0.04–0.16 wt%), Ti (127–476 ppm), and CaO (0.53–0.92 wt%) than the Laochang granites (Fig. 4). The Kafang granites show nearly flat patterns with significant negative Eu anomalies ($(La/Yb)_N$ = 0.68–6.50; Eu/Eu* = 0.01–0.06; Fig. 5a) in the chondrite-normalized REE patterns. The Kafang granitic samples have similar trace element patterns to the Laochang granites with higher degree of enrichment in Li, Rb, Y, Ta, U and depletion in Sr, Ba (Fig. 5b). They exhibit similar Nd-Hf-O isotopic compositions to the Laochang granites (−9.0 to −7.7, −8.8 to −6.1, 7.45–9.74‰, respectively) (Sun et al., 2023). Both the Laochang and Kafang granites are highly fractionated

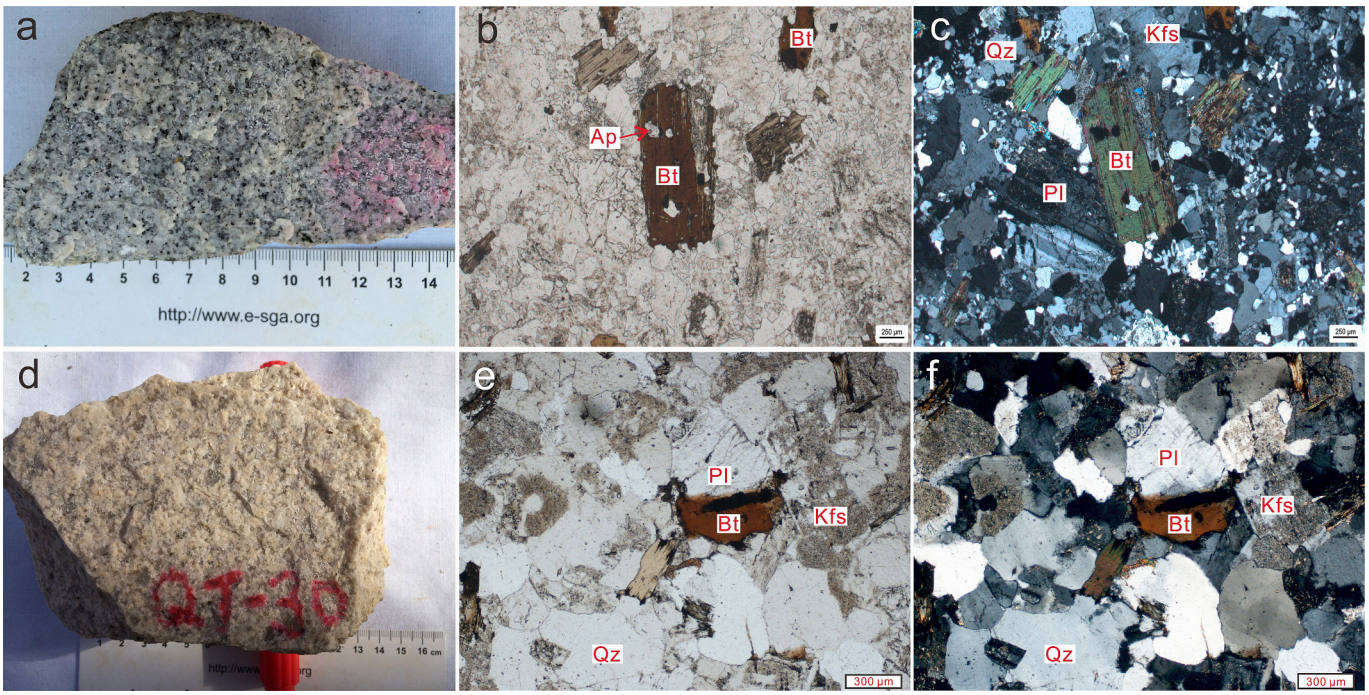

Fig. 3. Representative specimen and photomicrographs of the Laochang and Kafang granite. (a) Laochang fine-grained two-mica equigranular granite; (b-c) Microphotography of Laochang granite with phenocrysts of biotite, plagioclase, K-feldspar, apatite, and late-stage quartz; (d) Equigranular texture of the Kafang granite with minor mafic minerals; (e-f) Microphotography of Kafang granite composed of biotite, K-feldspar, plagioclase, and quartz.
Abbreviations: Ap = apatite, Bt = biotite, Kfs = K-feldspar, Pl = plagioclase, Qz = quartz, Pl = plagioclase.

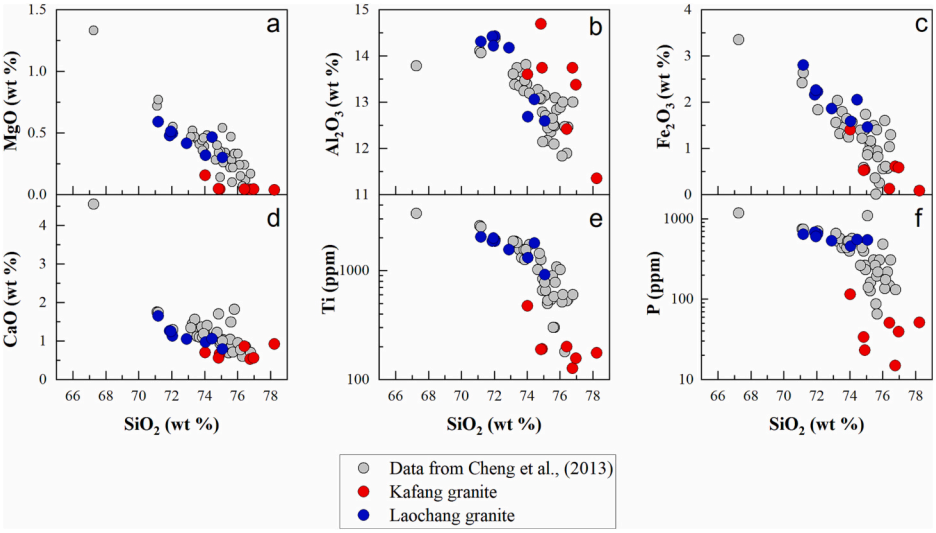

Fig. 4. Harker diagrams for the Laochang and Kafang granites in Gejiu district. Ore-related granite samples from Cheng et al. (2013b) are also shown.

granite given by their lower K/Rb, Nb/Ta, and Zr/Hf ratios than those of less fractionated granitic rocks (Fig. 5c and d).

3. Analytical methods

3.1. Whole-rock fluorine and chlorine contents analysis

F and Cl concentrations of the bulk rock samples were analyzed at ALS Laboratory Group (Guangzhou, China). Approximately 500 mg powdered samples were first mixed with KOH and MgO at a mass ratio of 1:3:1, and subsequently fused in an electric furnace at 900 °C for 40 min. The fused samples were dissolved and fluorine concentration was determined using a F-ELE81a Ion Selective Electrode (ISE, XL500, Accumet) and chlorine content was analyzed using Ion Chromatography (IC, IC930, Metrohm). Detection limits for F and Cl are 20 and 50 ppm, respectively. Analytical uncertainty is <10%. The standards JR-1 processed as unknown samples during this study, yielding F and Cl contents of 980 ppm and 930 ppm, respectively, consistent with the recommend values (1011 ± 28 ppm of Fe and 898 ± 26 ppm of Cl; Shimizu et al., 2006).

3.2. Whole-rock Sn isotope analysis

The Sn isotope analysis of whole-rock samples was conducted at the State Key Laboratory for Mineral Deposits Research, Nanjing University, China. The sample dissolution, chemical purification and analytical

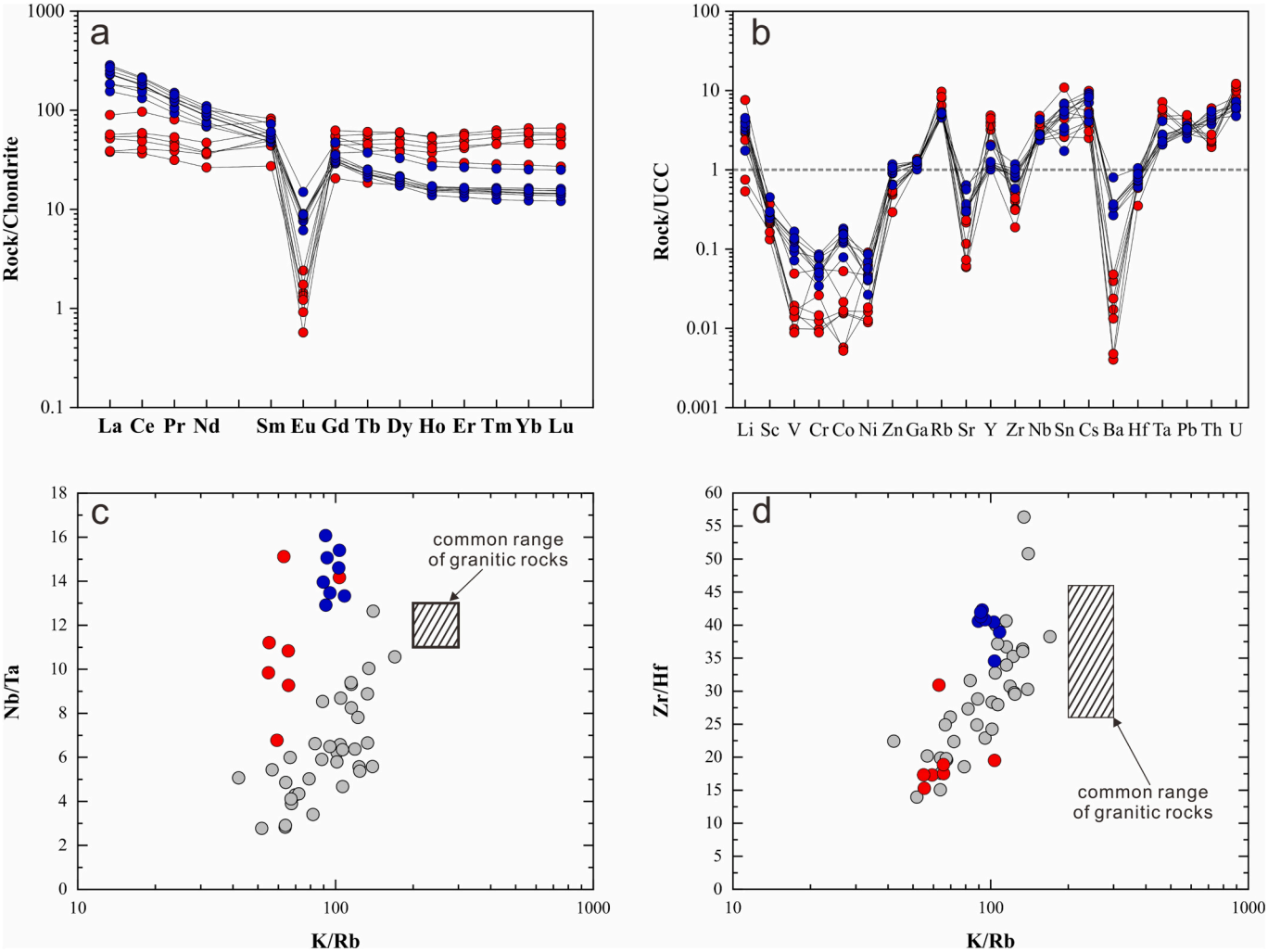

Fig. 5. Trace elemental compositions of the Laochang and Kafang granite. (a) Chondirite-normalized REE patterns; (b) Upper continental crust-normalized trace element diagrams; (c) Plot of K/Rb vs. Nb/Ta; (d) Plot of K/Rb vs. Zr/Hf. The normalization values of chondirite and UCC are from Sun and McDonough (1989) and Rudnick and Gao (2003), respectively. The ranges of common granitic rocks are from Jahn et al. (2001). Data of other ore-related granites are from Cheng et al. (2013a). See Fig. 4 for symbols used.

procedures followed those described by She et al. (2023b). Approximately 100 mg of sample powder and a corresponding amount of ^{117}Sn—^{122}Sn double spike solution with an optimal spike-to-sample ratio of 39:61 were weighed in Teflon beakers. The sample-spike mixture was digested with 8 mL 1:1 mixture of HNO_3-HF on a hotplate at 130 °C for two days. After repeated evaporation using aqua regia and HCl to obtain complete dissolution, these final solutions were dissolved in 0.5 M HCl for chemical separation of Sn. About 100 μL HF was added to the beaker before each evaporation step to prevent Sn loss by volatilization or hydrolysis. Tin was purified using 1.5 mL Eichrom TRU resin conditioned with 0.5 M HCl and matrix elements were eluted with 0.5 M and 0.25 M HCl sequentially. 100 μL HF was added to the collection beaker to prevent Sn hydrolysis before the collection of Sn cut. Then Sn was recovered using an eluent of 12 mL 0.5 M HNO_3. The purified Sn fractions were dried down at 80 °C and were brought up in a mixture acid of 0.3 M HNO_3 –0.006 M HF.

Tin isotope ratios were analyzed using a Nu 1700 Sapphire MC-ICP-MS at State Key Laboratory for Mineral Deposits Research and Frontiers Science Center for Critical Earth Material Cycling, Nanjing University. Tin solutions were diluted to 100 ppb for analysis and bracketed with a spiked NIST 3161a standard solution at the same concentration. Isotope measurements were performed in static mode using standard Ni cones with the ^{120}Sn sensitivity of >15 V/ppm. Tin isotope ratios are expressed as $\delta^{122/118}Sn$ notation relative to Sn isotopic standard solution NIST 3161a: $\delta^{122/118}Sn = [(^{122}Sn/^{118}Sn)_{sample} / (^{122}Sn/^{118}Sn)_{3161a}-1] \times 1000$. The standards GSP-2, JG-2, and GSP-1 processed as unknown samples during this study, yielded $\delta^{122/118}Sn$ values of 0.24 ± 0.03 (2SD, n = 3), 0.50 ± 0.03 (2SD, n = 3), 0.22 ± 0.02 (2SD, n = 3), respectively, consistent with those reported by recently studies (She et al., 2023a; Wang et al., 2022; She et al., 2023b).

4. Results

Whole-rock F and Cl contents, Sn isotopic values, and other related geochemical data are listed in Table 1. The F, Cl, and F/Cl rations of the Laochang granites vary from 1160 to 2380 ppm, 250 to 360 ppm, and 4.64 to 6.61, respectively. The Kafang granites have higher contents of F (790–3640 ppm), lower Cl concentrations (140–190 ppm), and a wider range of F/Cl ratios (4.16–26) compared to the Laochang granites. Both the Laochang and the Kafang granites show heterogeneous Sn contents, with ranges of 3.63–14.2 ppm and 5.44–22.9 ppm, respectively. The samples from the Laochang granite have $\delta^{122/118}Sn$ values ranging from 0.13 ± 0.04‰ to 0.43 ± 0.03‰, and those from the Kafang granite have $\delta^{122/118}Sn$ values varying from 0.11 ± 0.02‰ to 0.93 ± 0.02‰ (Fig. 6). One Kafang granite sample (QJ-23) yielded the highest Sn content (22.9 ppm) and lowest Sn isotope composition (0.11 ± 0.02‰, 2SD)

Table 1
Whole-rock Sn isotope compositions for the Laochang and Kafang granites in the Gejiu district.

Sample No	Locality	$\delta^{122/118}$Sn (‰)	2σ	SiO_2	CaO	$Fe_2O_3^T$	LOI	Sn	Nb	Ta	Ti	Cs	Th	F	Cl	Eu/Eu*	$\varepsilon_{Nd}(t)$
				Major element compositions (wt%)				Trace element compositions (ppm)									
ZYS-16	Laochang	0.35	0.04	75.08	0.79	1.46	0.76	6.36	28.8	1.87	921	20.0	39.8	1160	250	0.19	−8.8
ZYS-26	Laochang	0.43	0.03	74.05	0.97	1.58	1.04	10.5	31.6	2.37	1312	45.3	39.5	1220	260	0.16	−9.0
ZYS-27	Laochang	0.41	0.03	72.91	1.05	1.86	0.74	11.6	29.3	2.00	1557	39.5	47.2	1500	300	0.20	−8.8
ZYS-28	Laochang	0.13	0.04	71.19	1.65	2.80	1.01	3.63	51.7	3.70	2044	25.0	44.1	2380	360	0.26	−8.3
ZYS-29	Laochang	0.36	0.05	74.44	1.06	2.05	0.69	10.3	28.3	1.88	1789	34.5	47.1	1570	310	0.23	−8.8
ZYS-30	Laochang	0.31	0.04	72.05	1.13	2.22	0.79	14.2	33.9	2.51	1863	41.1	49.1	1810	330	0.21	−8.9
ZYS-31	Laochang	0.39	0.04	71.89	1.26	2.16	1.16	7.15	32.2	2.50	1866	43.0	52.4	1800	300	0.20	−9.0
ZYS-32	Laochang	0.38	0.03	71.96	1.25	2.26	0.92	11.5	33.0	2.05	1994	40.6	57.8	1910	320	0.19	−8.9
QJ-23	Kafang	0.48	0.04	74.92	0.67	0.54	0.61	5.44	28.4	2.01	190	18.1	21.2	790	190	0.06	−8.3
QJ-25	Kafang	0.64	0.01	76.77	0.53	0.60	0.69	11.2	44.4	3.96	127	22.6	20.3	1200	170	0.01	−7.7
QJ-26	Kafang	0.57	0.04	76.97	0.56	0.58	0.61	9.34	43.6	6.43	156	23.0	23.7	1480	170	0.03	−8.3
QJ-28	Kafang	0.93	0.02	74.03	0.70	1.40	0.66	14.4	35.7	2.36	476	48.5	62.8	2900	180	0.04	−8.3
QJ-29	Kafang	0.60	0.03	74.85	0.56	0.53	0.65	13.6	41.8	4.25	189	27.1	23.9	1520	160	0.02	−8.9
QJ-30	Kafang	0.43	0.04	78.24	0.92	0.08	0.94	5.51	46.8	5.05	176	12.3	25.0	3640	140	0.02	−9.0
QJ-31	Kafang	0.11	0.02	76.41	0.86	0.12	0.96	22.9	57.3	5.29	200	14.9	29.3	2820	140	0.02	−8.3
GSP-2	Standard	0.24	0.03														
JG-2	Standard	0.50	0.03														
GSP-1	Standard	0.22	0.02														

Notes: The major, trace elements and Nd isotopic data of the Laochang and Kafang granites are from Xu et al. (2022b) and Sun et al. (2023), respectively.

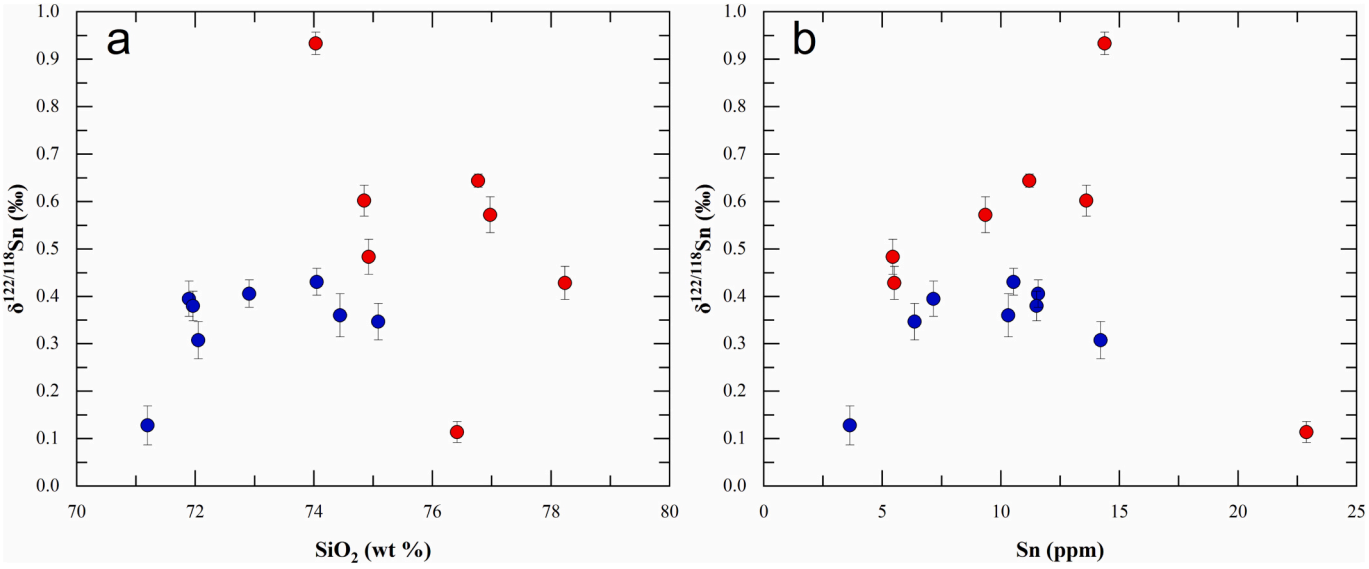

Fig. 6. Variations of $\delta^{122/118}$Sn with SiO_2 (a) and Sn (b) contents. See Fig. 4 for symbols used.

compared with other Kafang granite samples (Fig. 6b). The Sn isotopic values of the Kafang granites are higher than the Laochang granites except for that outlier. The $\delta^{122/118}$Sn values of the Laochang granitic rocks show negative correlation with CaO, $Fe_2O_3^T$, Ti, and Eu/Eu*, while the Kafang samples display a broad scatter (Fig. 7).

5. Discussion

5.1. The role of hydrothermal alteration, wall-rock assimilation, and source heterogeneity in Sn isotope fractionation

All granite samples studied are fresh without obvious signs of alteration in both hand specimen and thin section, and have low LOI values (≤1.2 wt%; Table 1). The LOI values of granites are not correlated with either Sn contents or $\delta^{122/118}$Sn values, indicating the influence of hydrothermal alteration on Sn isotopes is insignificant (Fig. 8a, b). However, one Kafang granite sample (QJ-23) shows obvious low $\delta^{122/118}$Sn value of 0.11 ± 0.02‰ than the other samples (Fig. 6). This low value may be attributed to the formation of minor hydrothermal cassiterite, which is in line with the following observations: (1) this sample (QJ-23) yielded the highest Sn content among all the samples; (2) the low $\delta^{122/118}$Sn value is close to the reported cassiterite $\delta^{122/118}$Sn value of 0.13‰ (recalculated relative to NIST SRM 3161a) from the Gejiu ore district (Liu et al., 2021; Yamazaki et al., 2013).

Wall-rock assimilation and source heterogeneity are also possible processes that can modify the Sn isotope compositions of granitic melts. However, they are unlikely to account for the observed Sn isotope variability in the Gejiu granites based on the following lines of evidence: (1) these granite samples are homogeneous and free of country rock (carbonate) xenocrysts or residue minerals; (2) they exhibit homogeneous and similar Nd-Hf-O isotopic compositions, with no correlations between ε_{Nd} (t) values and SiO_2 or Nd contents (Xu et al., 2022b; Sun et al., 2023); (3) there is no correlations between ε_{Nd} (t) values and Sn contents or $\delta^{122/118}$Sn values (Fig. 8c, d). The Laochang granites show an apparent negative relationship between Nd and Sn isotopes (Fig. 8d), but the trend was controlled by only one sample that had low $\delta^{122/118}$Sn value and high ε_{Nd} values, and the rest of samples are essentially identical considering the external uncertainties in the analyses of Sn (0.03‰ in $\delta^{122/118}$Sn) and Nd isotopes (±0.5 in ε_{Nd}).

Crustal anatexis processes can fractionate metal isotopes between the

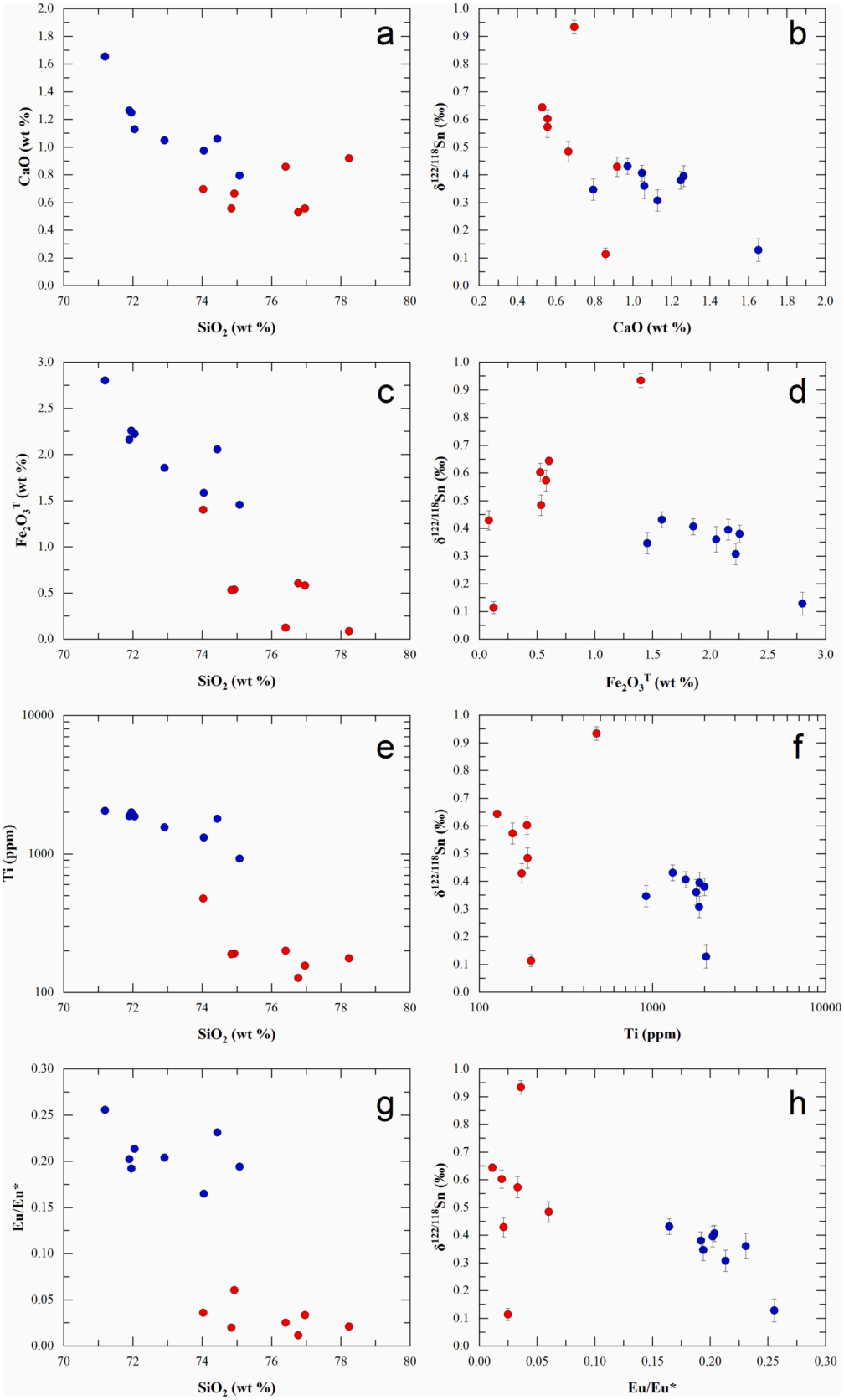

Fig. 7. Representative magmatic differential indices and their relationships with Sn isotopes for the Laochang and Kafang granites. (a) plot of SiO_2 vs. CaO; (b) plot of CaO vs. $\delta^{122/118}Sn$; (c) plot of SiO_2 vs. $Fe_2O_3^T$; (d) plot of $Fe_2O_3^T$ vs. $\delta^{122/118}Sn$; (e) plot of SiO_2 vs. Ti; (f) plot of Ti vs. $\delta^{122/118}Sn$; (g) plot of SiO_2 vs. Eu/Eu*; (h) plot of Eu/Eu* vs. $\delta^{122/118}Sn$. See Fig. 4 for symbols used.

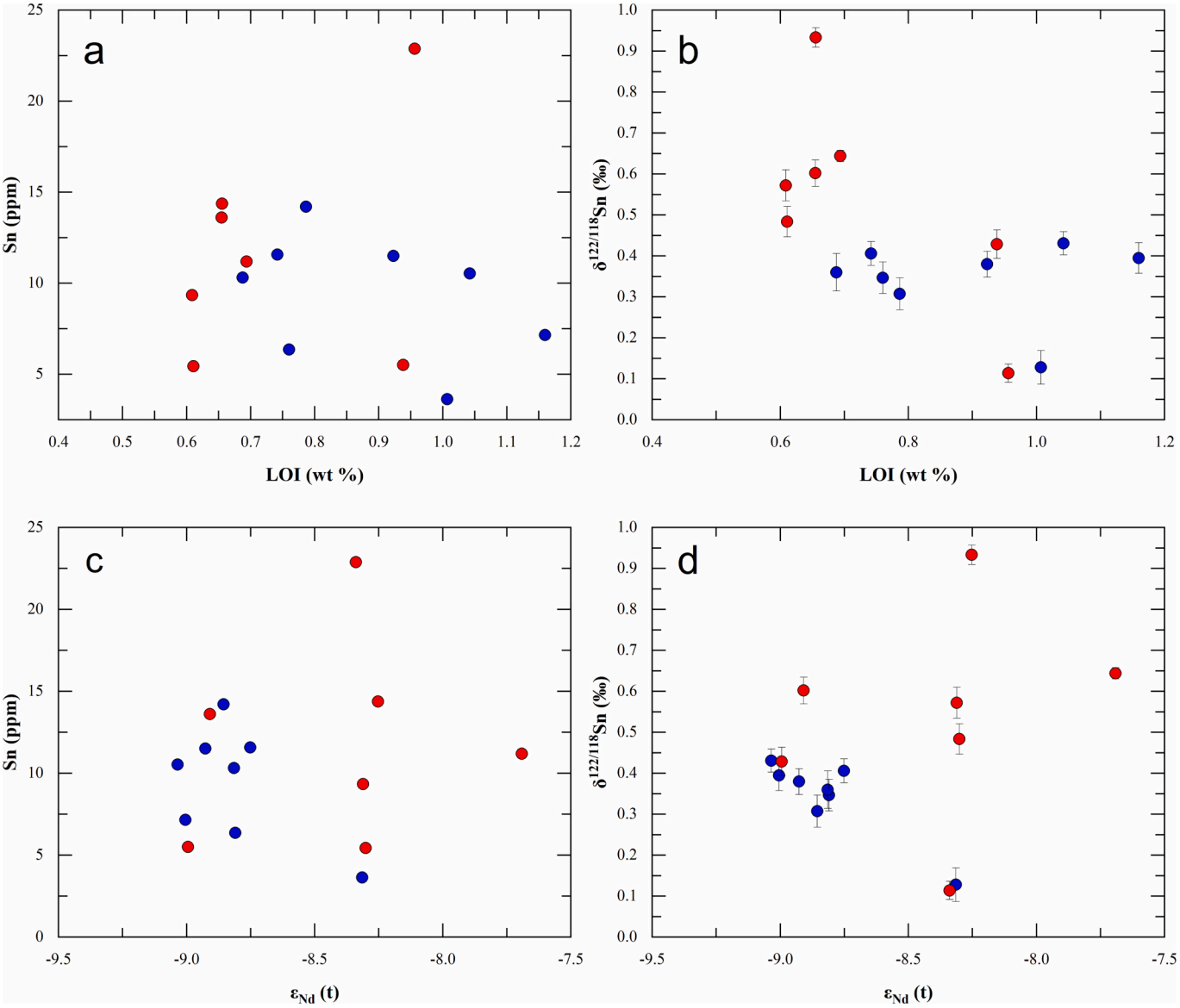

Fig. 8. (a) Plot of LOI vs. Sn for the Laochang and Kafang granites; (b) plot of LOI vs. $\delta^{122/118}$Sn; (c) plot of ε_{Nd}(t) vs. Sn; (d) plot of ε_{Nd}(t) vs. $\delta^{122/118}$Sn. The Nd isotope data of the Laochang and Kafang granites are from Xu et al. (2022b) and Sun et al. (2023). See Fig. 4 for symbols used.

melt and the residue, as been reported for several elements such as Li (Sun et al., 2016; Chen et al., 2020) and Fe (Telus et al., 2012; He et al., 2017). Tin isotopes can fractionate during mantle partial melting, with basalts enriched in heavy Sn isotopes relative to peridotite (Wang et al., 2018). This can be attributed to different partitioning behavior of Sn^{4+} and Sn^{2+} during partial melting given that Sn^{4+} is more incompatible and enriched in heavy isotopes relative to Sn^{2+} (Wang et al., 2018). However, the Sn isotopic behavior during partial melting of crustal rocks remains unknown. Based on the study of mantle partial melting, Sn isotopic fractionation during crustal anatexis could be mainly controlled by Sn speciation difference between melt and residue. Redox conditions and melt compositions are the two most important factors that affect Sn speciation in the melt (Farges et al., 2006; Linnen et al., 1996; Roskosz et al., 2020). Tin exists predominantly as Sn^{2+} in reduced peraluminous granitic magmas and it occurs as Sn^{4+} in oxidized peralkaline melts (Ishihara, 1977; Lehmann and Mahawat, 1989; Linnen et al., 1996). Experimental studies have shown that >90% of tin is present as Sn^{2+} in granitic magmas at oxygen fugacity lower than the Ni-NiO buffer (Durasova et al., 1986). Both the Laochang and Kafang granites have similar logfO_2 of △FMQ - 2.5 to △FMQ + 1.2 (△FMQ = −0.81 ± 0.84, n = 46; where FMQ is fayalite-magnetite-quartz) calcaulated using the method of Loucks et al. (2020) based on zircon trace element data (Xu et al., 2022b; Sun et al., 2023), with most values being less than FMQ, indicating Sn existed as Sn^{2+} in these melts. Considering the negligible amounts of Sn^{4+} within the above granitic magmas, crustal anatexis contributed little to Sn isotopic fractionation for these Sn-enriched reduced Gejiu granites. Thus, hydrothermal alteration, wall-rock assimilation, source heterogeneity and anatexis process cannot account for the Sn isotope fractionation within the Laochang and Kafang granites. The wide range of $\delta^{122/118}$Sn values in the Gejiu granites should reflect isotope fractionation during magmatic evolution processes including fractional crystallization and late-stage magmatic-hydrothermal fluids exsolution, which will be further discussed in detail below.

5.2. *Sn isotope fractionation during fractional crystallization and fluid exsolution processes*

The obvious negative correlations between SiO_2 and major elements (e.g., CaO, $Fe_2O_3^T$, TiO_2), along with the significant negative Eu

anomalies and depletion in Sr and Ba, indicate these granites have undergone strong crystal fractionation during magma ascent (Figs. 4 and 5). The separated minerals were dominantly by feldspars (10–35% plagioclase and 40–65% K-feldspar) and minor biotite (~10%) based on Rayleigh fractionation crystallization modeling of Rb, Sr, and Ba contents (Sun et al., 2023). As shown in Fig. 7, the Laochang granite samples show negative correlations between $\delta^{122/118}$Sn values and CaO, Fe_2O_3, Ti contents and Eu/Eu* ratios, indicating that low-$\delta^{122/118}$Sn components were removed during the evolution of these magmas. Previous studies proposed that removal of ilmenite in basaltic magma would decrease the $\delta^{122/118}$Sn values in the residual melt (Badullovich et al., 2017). However, this mechanism may not work for the Laochang granites due to their low Ti contents ($TiO_2 < 0.30$ wt%) and elevated Sn isotope trend with magma evolution (Fig. 7). As mentioned above, the crystallized minerals consist of plagioclase, K-feldspar, biotite, quartz, and minor accessory minerals such as zircon, apatite, and ilmenite (Fig. 4). Because of the low mineral-melt partition coefficients of Sn for K-feldspar and quartz (Kd $\leq$ 0.05, Table 2), the behavior of Sn during fractional crystallization is mainly dictated by the proportions of plagioclase, biotite, and ilmenite (Simons et al., 2017; Zhao et al., 2022a). It is noteworthy that the Kafang granites are more evolved than the Laochang granites in terms of element concentrations, but the correlations between the magmatic differentiation indicators (e.g., Fe_2O_3, Ti, Eu/Eu*) and Sn isotopic values are not continuous (Fig. 7), which suggest other processes may also affect Sn isotope compositions of the Kafang granites in addition to crystal fractionation.

Tin is a fluid-mobile element and will preferentially partition into the fluid phase during fluid exsolution process at the end stage of highly evolved granitic magmas (Zhao et al., 2022a), which would decrease the Sn concentrations and lead to possible Sn isotope fractionation in the residual melt. Tin mineralization in Gejiu deposit is genetically related to magmatic-hydrothermal fluids derived from highly evolved granitic magmas (Cheng et al., 2013a; Xu et al., 2022a; Sun et al., 2023). Here, we evaluate the effect of fluid exsolution on Sn isotope compositions of the Gejiu granites. We use the whole-rock F/Cl ratios to trace the fluid exsolution process. Variations of F/Cl ratios in magmas are sensitive to the timing and/or degree of fluid exsolution and fractionated minerals. As a general rule, Cl is strongly partitioned into fluid over a melt during exsolution of a hydrous magmatic volatile phase, whereas F will preferentially partition into melt (Zhu and Sverjensky, 1991; Rasmussen and Mortensen, 2013). The partition coefficients of F and Cl between magmatic hydrothermal fluids and highly evolved granitic magmas are <0.4 and ~ 37, respectively (Webster and Holloway, 1990). This means that fluid exsolution will elevate the F/Cl ratios in the residual melts. In a magma that has not experienced fluid exsolution, removal of hydrous minerals (e.g., biotite and apatite) will decrease the F/Cl ratios of residual melts because F is more compatible than Cl in these minerals. The $D_{F/Cl}$ (where D is the mineral-melt partition coefficient) is ~1.9 for biotite (Icenhower and London, 1997), and ~8.5 for apatite (Webster et al., 2009). Thus, fluid exsolution will significantly increase the F/Cl ratios of the residual melts, whereas fractional crystallization will lead to an opposite trend. As shown in Fig. 9a, the Laochang granites exhibit negative correlation between SiO_2 contents and F/Cl ratios, suggesting the magma at this stage was not fluid-saturated and it was dominantly controlled by fractional crystallization. Analogous to the correlations between magmatic differentiation indices and Sn isotopes for the Laochang granites (Fig. 7), the F/Cl ratios are also negatively related with the Sn isotopic values, indicating fractional crystallization would increase the Sn isotopic values in the residual magmas (Fig. 9b). Compared with the Laochang granites, the Kafang granites show higher SiO_2 contents, F/Cl ratios, and overall higher $\delta^{122/118}$Sn values, suggesting the magma at this stage was fluid-saturated and fluid exsolution coupled with fractional crystallization would further enrich the heavy Sn isotopic values in the residual melt (Fig. 9). Therefore, both the fractional crystallization and fluid exsolution are important mechanisms that controlled the Sn isotope fractionation in Gejiu granites.

Table 2
Partition coefficients used for fractionation crystallization modeling.

Minerals	Qtz	Kfs	Pl	Bt	Ilm	Fluid
D_{Sn}	0	0.05	0.6	2.32	5	7
D_{Nb}	0	0	0	3.6	73	0
D_{Ta}	0	0	0	1.2	86	0

Notes: Abbreviations: Bt = biotite, Ilm = ilmenite, Kfs = K-feldspar, Pl = plagioclase, Qtz = quartz.
The partition coefficients D_{Sn} are from Simons et al. (2017); D_{Nb} and D_{Ta} are from Nash and Crecraft (1985). The partition coefficients D_{Sn} for ilmenite and fluid are from Badullovich et al. (2017) and Zhao et al. (2022b), respectively.

5.3. Quantitative assessment of Sn isotope fractionation in a crystal-melt-fluid system

5.3.1. Fractionation model in crystal-melt system for the Laochang granites

As discussed before, the Laochang granitic samples are fluid-unsaturated and fractional crystallization is the dominant mechanism during magma evolution, providing a chance to quantitatively evaluate the effect of crystal fractionation alone on Sn isotope fractionation. We performed Rayleigh fractionation modeling for the Laochang granites, and the Sn contents and isotope values of residual melts are calculated as follows:

$$Cm = Ci\ m \times F_m^{Kcm-1} \quad (1)$$

$$\delta^{122/118}Sn_m = \left(\delta^{122/118}Sn_i + 1000\right) \times f^{(\alpha 1-1)} - 1000 \quad (2)$$

where.

Ci m = content of Sn in the initial melt,
F_m = mass fraction of melt,
Kcm = bulk crystal-melt partition coefficient,
$\delta^{122/118}Sn_i$ = Sn isotope of the initial melt,
$\delta^{122/118}Sn_m$ = Sn isotope of the melt,
α1 = the Sn isotope fractionation factor between crystal and melt,
f = the fraction of Sn remaining in the melt.

The least evolved granite sample ZYS-28, which has highest Ca, Fe, Ti, Eu/Eu*, and F/Cl values and lowest Si and Sn contents and Sn isotope ratio ($\delta^{122/118}$Sn = 0.13), was used as the initial melt composition (Figs. 6, 7, 9; Table 1). From the equations listed above, Sn isotope of residual melt is affected by two parameters including Kcm and α1. Bulk crystal-melt partition coefficient (Kcm) of Sn between separated minerals and melt is mainly controlled by the fractions of plagioclase, biotite, and ilmenite. As suggested by Sun et al. (2023), the magma contained 10–35% plagioclase during crystal fractionation, contributing to 0.06–0.21 for the Kcm (Table 2). In order to constrain the proportions of biotite and ilmenite during crystal fractionation, we carried out Rayleigh fractionation modeling using Nb and Ta given that these two elements are mainly hosted in biotite and ilmenite in reduced highly differentiated S-type granitic magmas (Stepanov et al., 2014; Sun et al., 2019). Rayleigh fractional crystallization modeling suggests that the Laochang granites can be formed by 40–60% crystallization with 5–15% biotite and 2% ilmenite assuming the least evolved sample as the initial melt composition (Fig. 9c and d). In contrast, the Kafang granites are consistent with 50–80% crystallization with 15–25% biotite (Fig. 9c and d). To date, no partition coefficient has been reported for Sn^{2+} between ilmenite and felsic magmas. We assume Dilmenite Sn of 5 based on calculated partition coefficient of 4.5–6.8 for Sn^{4+} using lattice strain theory (Badullovich et al., 2017). Considering the lower compatibility of Sn^{2+} and the minor amounts of ilmenite, ilmenite crystallization contributed to <0.1 for the bulk crystal-melt partition coefficient. Based on the above discussions, the calculated bulk crystal-melt partition coefficient is in the range of 0.18 to 0.66 for the Laochang granites (Table 2). Experimental data of Sn isotope fractionation factor $\triangle^{122/}$

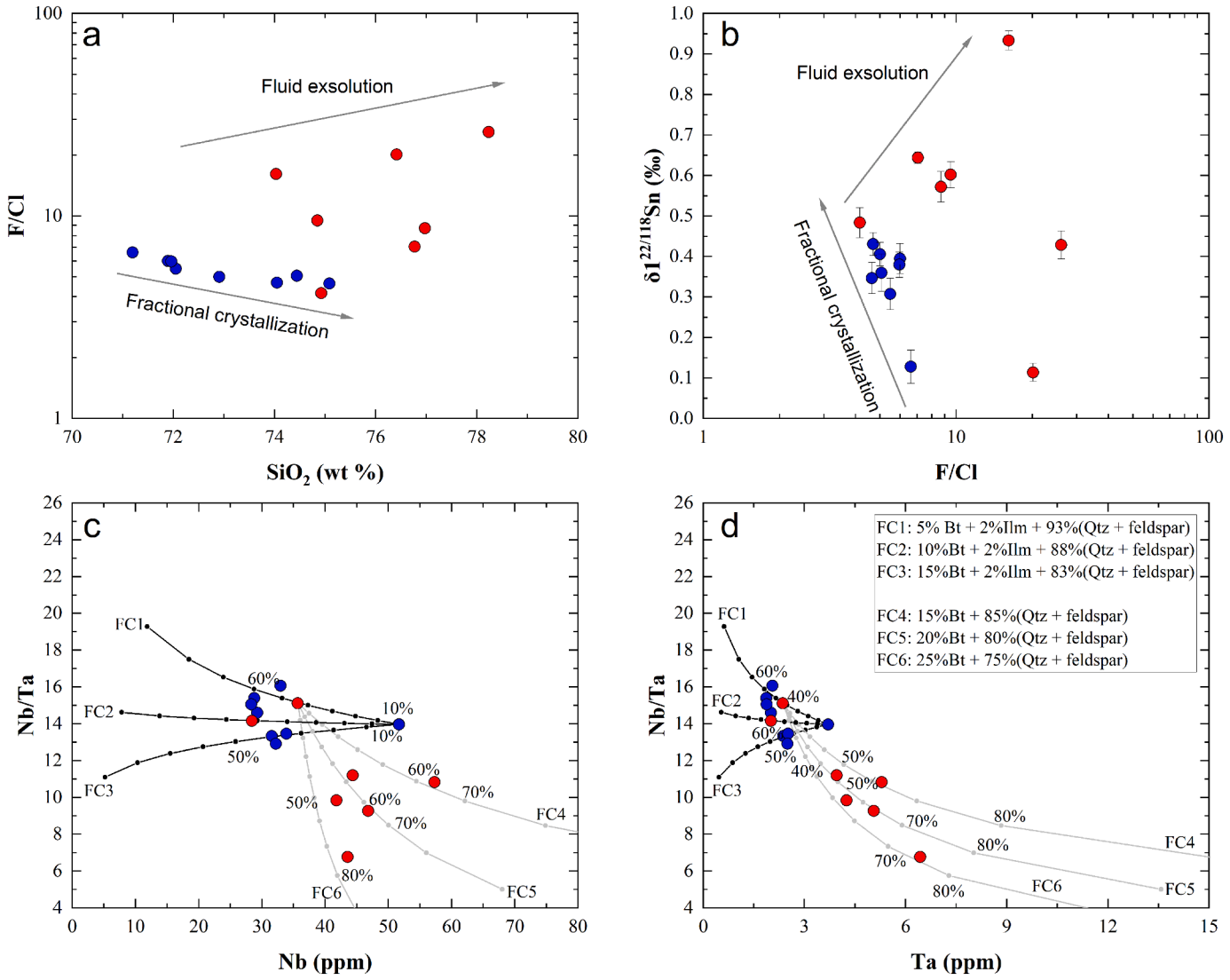

Fig. 9. (a) Plot of SiO_2 vs. F/Cl for the Laochang and Kafang granites; (b) diagram showing variation in F/Cl versus $\delta^{122/118}Sn$; (c-d) Nb/Ta versus Nb and Ta contents for the Laochang and Kafang granites. Solid curves represent evolution trend of the different minerals assemblages using the Rayleigh distillation law, the number on the diagram refer to the degree of fractional crystallization. The partitioning coefficients used for modeling are given in Table 2. See Fig. 4 for symbols used.

$^{118}Sn_{crystal\text{-}melt}$ in a S-type granitic melt are presently not available. Taking into account the increased trend between Sn isotopes and magma differentiation indices, we calculated the Sn isotopes of residual melts based on eq. (2) assuming $\triangle^{122/118}Sn_{crystal\text{-}melt}$ values in the range of −1 to −0.1‰. Combined with the bulk crystal-melt partition coefficient discussed above, our calculation indicates that $\triangle^{122/118}Sn_{crystal\text{-}melt}$ = −0.6 to −0.5‰ would yield the observed $\triangle^{122/118}Sn$ values of the Laochang granites (Fig. 10). Thus, we recommend that the Sn isotope fractionation factor $\triangle^{122/118}Sn_{crystal\text{-}melt}$ could be ~ −0.5‰ for the reduced S-type granitic system.

5.3.2. *Fractionation model in crystal-melt-fluid system for the Kafang granites*

Compared with the fluid-unsaturated Laochang granitic magmas, the magmas for the Kafang granites underwent further fluid saturation and exsolution. Thus, both crystal fractionation and magmatic-hydrothermal exsolution could have affected the Sn isotope variations of the Kafang granites. Here, we model Sn contents and Sn isotopic compositions in a crystal-melt-fluid system for the Kafang granites. The Sn content within a residual melt after water saturation can be calculated using the equation proposed by Spera et al. (2007), and the Sn isotopic ratio was calculated following Fan et al. (2022) for Mo isotope as follows:

$$Cm = Cs\,m\left(\frac{F_m}{F_m^s}\right)^{K_{cm}\left(1-\frac{K_{fm}}{K_{cm}}\right)\Phi H2O+Kcm-1} \quad (3)$$

$$\delta^{122/118}Sn_m = \left(\delta^{122/118}Sns\,m + 1000\right)\times f^{'(\alpha 2-1)} - 1000 \quad (4)$$

$$f^{'} = Fm \times \left(\frac{C_m}{C_m^0}\right) \quad (5)$$

where.

Cs m = content of Sn in the melt at water saturation,

F_m = mass fraction of melt,

Fs m = mass fraction of melt at water saturation,

K_{cm} = bulk crystal-melt partition coefficient,

K_{fm} = bulk fluid-melt partition coefficient,

ΦH_2O = negative value of the solubility of water in the melt,

$\delta^{122/118}Sns\ m$ = Sn isotope of melt at water saturation,

α2 = the Sn isotope fractionation factor between (crystal + fluid) and melt,

$f^{'}$ = the fraction of Sn remaining in the melt.

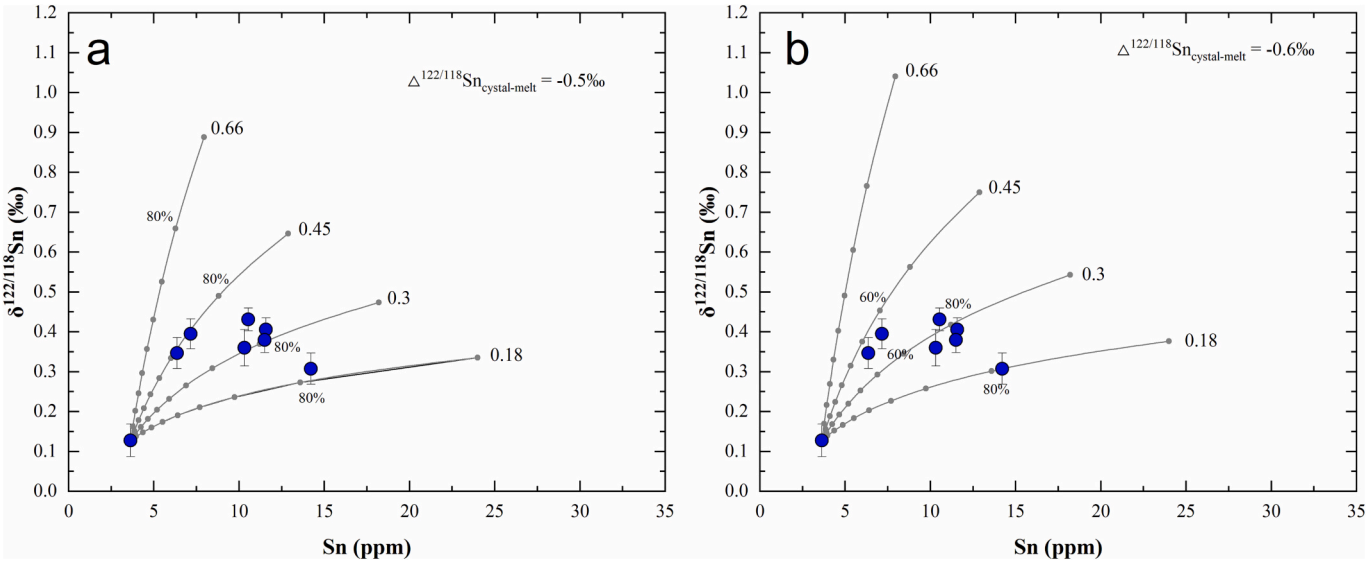

Fig. 10. Rayleigh fractionation models for whole-rock Sn contents and Sn isotopes before water-saturation for the Laochang granites with $\triangle^{122/118}Sn_{crystal\text{-}melt}$ of −0.5‰ (a) and $\triangle^{122/118}Sn_{crystal\text{-}melt}$ of −0.6‰ (b).

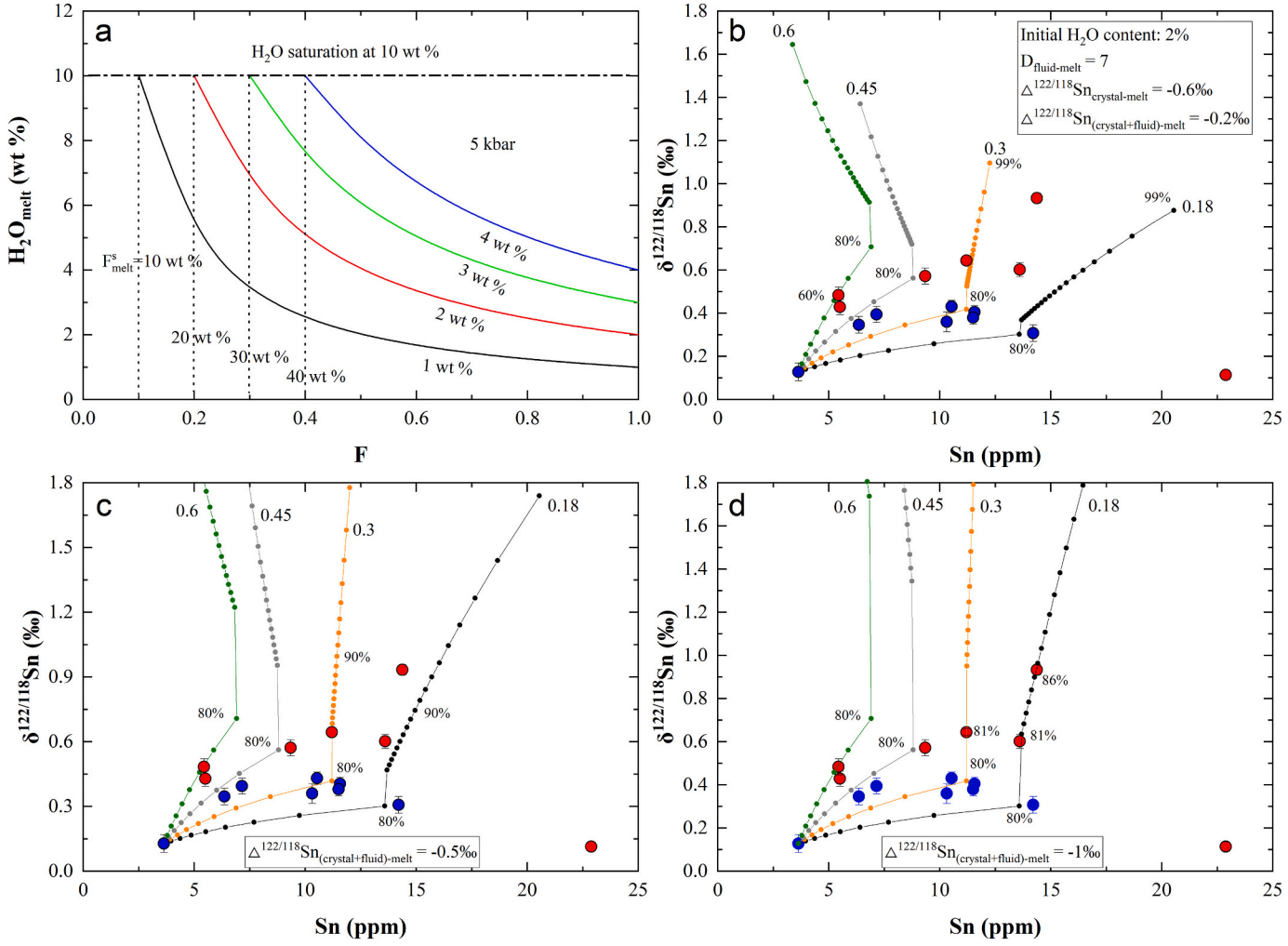

Fig. 11. (a) Diagram showing the predicted H_2O contents evolution of residual melts with different initial H_2O contents. H_2O is regarded as a perfect incompatible component element and water solubility was calculated from the equation of Holtz et al. (2001); (b-d) Rayleigh fractionation models for whole-rock Sn contents and Sn isotopes with different $\triangle^{122/118}Sn_{(crystal+fluid)\text{-}melt}$ values. The number on the colored curves refer to the different bulk crystal-melt partition coefficients (K_{cm}) and the percentage data denote the degree of fractional crystallization.

The least evolved granite sample ZYS-28 with the lowest Sn content and $\delta^{122/118}Sn$ value (Sn = 3.63 ppm; $\delta^{122/118}Sn$ = 0.13‰) was used as the initial melt composition. The complicated modeling should first constrain the following parameters: the bulk crystal-melt partition coefficient (K_{cm}), the bulk fluid-melt partition coefficient (K_{fm}), solubility of water in the melt (-ΦH_2O), mass fraction of melt at water saturation (Fs m), and the Sn isotope fractionation factor between separated phases (crystal + fluid) and melt (α2). As suggested above, the K_{cm} ranges from 0.18 to 0.66 (Fig. 10). Experimental results and fluid inclusion studies yielded a large range in the Sn fluid-melt partition coefficient (K_{fm}=0.3–42) (Audétat, 2019; Zajacz et al., 2008). The K_{fm} of Sn is mainly correlated with the melt composition (especially the aluminium saturation index ASI) and the Cl concentration in the fluid (Zhao et al., 2022b). Combined with the whole-rock results and primary fluid inclusion salinity data from Kafang deposit (Cheng et al., 2012; Sun et al., 2023), we calculated an average K_{fm} value of 7 for the magmatic-hydrothermal fluid based on the equation of Zhao et al. (2022b). The next step is to constrain the solubility of water in the melt, which is related to the crystallization pressure of the melt. The Kafang granitic magma was estimated crystallized at 5 kbar (using the biotite thermobarometer; Li and Zhang (2022)), corresponding to a water solubility (-ΦH_2O) of 10% based on the empirical equation of Holtz et al. (2001). We assume a wide range of initial H_2O contents (1-4 wt%) for the modeling of Kafang granitic magmas. H_2O is assumed as completely incompatible with respect to the crystallized minerals as the amount of H_2O hosted in hydrous minerals is negligible (<0.6 wt% for felsic igneous magmas; Caricchi and Blundy (2015)). In this way, we can constrain the mass fraction of melt at water saturation (Fs m) with different initial H_2O contents (Fig. 11a). A $\triangle^{122/118}Sn_{crystal\text{-}melt}$ value of −0.6‰ was used prior to fluid saturation, which is based on the modeling results for the Laochang granites (Fig. 10). The Sn isotope fractionation factor between melts and fluids is unclear. In this study, we assume a wide range of −1 to −0.2‰ for the $\triangle^{122/118}Sn_{(crystal+fluid)\text{-}melt}$ value for the modeling after fluid saturation (Figs. 11b-11d). The modeling results suggest $\triangle^{122/118}Sn_{(crystal+fluid)\text{-}melt}$ = −1–−0.5‰ with an initial H_2O content of 2 wt% can explain the observed $\delta^{122/118}Sn$ values of the Kafang granites (Figs. 11c-11d). A higher $\triangle^{122/118}Sn_{(crystal+fluid)\text{-}melt}$ value (−0.2‰) will need extreme degree of fractionation (>90%), which is not common for magmas with high SiO_2 contents. Besides, modeling results with lower (1 wt%) or higher initial water contents (≥3 wt%) are not consistent with the variation trends of the Sn isotopes of these granites (Fig. S1). In order to further constrain the Sn isotope fractionation factor between fluid and melt ($\triangle^{122/118}Sn_{fluid\text{-}melt}$), we calculated this value based on mass balance as follows:

$$\triangle^{122/118}Sn_{(crystal+fluid)-melt} = X_{crystal} \times \triangle^{122/118}Sn_{crystal-melt} + X_{fluid} \times \triangle^{122/118}Sn_{fluid-melt} \quad (6)$$

where $X_{crystal}$ and X_{fluid} are the mass fractions of Sn in crystals and fluid, respectively, with $X_{crystal} + X_{fluid} = 1$. The Sn content of the fractionated crystals and exsolved fluid can be calculated by $C_{crystal} = K_{cm} \times C_m$ and $C_{fluid} = K_{fm} \times C_m$, respectively. The mass ratio of separated crystals to the exsolved fluid is 90/10 as the crystallization of each 1 wt% of melt requires the release of 0.10 wt% fluid to maintain a water solubility of 10 wt% in the residual melt. Based on the K_{cm} = 0.18–0.45, K_{fm} = 7, $\triangle^{122/118}Sn_{crystal\text{-}melt}$ = −0.6–-0.5‰, and $\triangle^{122/118}Sn_{(crystal+fluid)\text{-}melt}$ = −0.5–-1‰ discussed above (Fig. 11), the calculated Sn isotope fractionation factor between fluid and melt ($\triangle^{122/118}Sn_{fluid\text{-}melt}$) is in the range of −1.9 to −0.7‰. The estimated fractionation between fluid and granitic melt is consistent, in direction, with theoretical predictions based on experimental synchrotron nuclear resonant inelastic X-ray scattering (NRIXS) data and first principles calculations (Roskosz et al., 2020; Wang et al., 2021), which show that the $1000ln^{122/116}\beta$ values of Sn(II)-Cl hydrothermal fluid are lower than those of reduced rhyolite glass at 500–700 °C. The magnitude of Sn isotope fractionation modeled in this study (−1.9 to −0.7‰ in $\triangle^{122/118}Sn_{fluid\text{-}melt}$) is greater than the theoretically predicted values (−0.3 to −0.2‰ in $\triangle^{122/118}Sn_{fluid\text{-}melt}$), which may be caused by the compositional difference between the Gejiu granite and experimental rhyolite glass of Roskosz et al. (2020). Accurate fractionation factors between Sn-bearing hydrothermal fluid and granitic magmas needs to be experimentally constrained in the future.

5.4. Origin of the mineralization-related hydrothermal fluids

The hydrothermal fluids associated with Sn mineralization may be generated by internal fluids exsolved from the highly evolved granitic magmas or exotic fluids contributed from the deep magma reservoirs (Deng et al., 2022). Based on the lower $\delta^{138/134}Ba$ and higher Pb content values in the latter-two stage highly differentiated granites from Qitianling batholith, Deng et al. (2022) proposed that the magmatic hydrothermal fluids responsible for Sn-polymetallic mineralization originated from the deep crystal mush rather than exsolved from highly evolved magma itself. However, this deep magmatic fluids model is not applicable to the Gejiu granites. Considering cassiterite is the major Sn-host minerals precipitated from hydrothermal fluids in Sn ore deposit and its Sn isotopes can roughly represent the isotopic composition of the hydrothermal fluids under scenario of quantitative Sn precipitation. We can't immediately evaluate the effect of the hydrothermal fluids on Gejiu granites due to the absence of high quality cassiterite Sn isotopic data. Wu et al. (2023) compiled cassiterite Sn isotopic data worldwide and found that their $\delta^{122/118}Sn$ values range from −0.82‰ to 0.91‰ with mean and median values at 0.24‰ and 0.21‰, respectively. Previous studies have identified large Sn isotopic variations in cassiterite during fluid evolution (Yao et al., 2018; Liu et al., 2021; Zhou et al., 2022). Thus, the statistical mean values of cassiterite is more likely to approximate the Sn isotopic composition of the hydrothermal fluids than the extreme values. The mean/median $\delta^{122/118}Sn$ value of cassiterite is lower than the Gejiu granites and reported intermediate-felsic igneous rocks (Wu et al., 2023), indicating hydrothermal fluids might be enriched in light Sn isotopes relative to granitic magmas. As discussed above, both the theoretical calculation and cassiterite data suggest addition of low-$\delta^{122/118}Sn$ magmatic-hydrothermal fluids decrease the $\delta^{122/118}Sn$ values of the Kafang granites, which is opposite with the Kafang granites showing higher $\delta^{122/118}Sn$ values than those of less differentiated Laochang granites (Fig. 6). Therefore, the mineralization-related hydrothermal fluids at Gejiu deposit are exsolved from highly differentiated magmas rather than exsolved from deep magma reservoir. Both the crystal fractionation and fluid exsolution processes cause increase of $\delta^{122/118}Sn$ values in the residual melt, with an inferred isotope fractionation factor $\triangle^{122/118}Sn_{fluid\text{-}melt}$ is ~ −1.9–−0.7‰ for the Gejiu granites.

6. Conclusions

This study presents high-precision Sn isotope compositions of two Sn mineralization-related highly evolved S-type granites from world-class Gejiu Sn-polymetallic ore district, South China. These granites show a broad range of Sn isotope values from 0.11‰ to 0.93‰. The $\delta^{122/118}Sn$ values of the Laochang granites show obviously negative correlations with indices of magmatic differentiation (e.g., contents of CaO, Fe_2O_3, Ti, and ratios of Eu/Eu* and F/Cl), which could be ascribe to the fractional crystallization of biotite, plagioclase, and minor ilmenite. The Kafang granites show higher SiO_2 contents, F/Cl ratios, and Sn isotopic compositions than those of the Laochang granites, suggesting the magma at this stage was fluid-saturated and fluid exsolution coupled with fractional crystallization would further enrich the heavy Sn isotopic values in the residual melt. Rayleigh fractionation modeling indicates that $\triangle^{122/118}Sn_{crystal\text{-}melt}$ = −0.6 to −0.5‰ and $\triangle^{122/118}Sn_{fluid\text{-}melt}$ = −1.9 to −0.7‰ with an initial H_2O content of 2 wt% can explain the observed $\delta^{122/118}Sn$ values of Gejiu granites. Our study implies that both the crystal fractionation and fluid exsolution processes control Sn isotope fractionation in the highly evolved granites and Sn isotopes are

useful for tracing the evolution details of highly differentiated igneous rocks.

CRediT authorship contribution statement

Ke-Ke Sun: Writing – original draft, Investigation, Funding acquisition, Conceptualization. **Jia-Xin She:** Writing – review & editing, Methodology, Investigation. **De-Hong Du:** Writing – review & editing, Investigation. **Weiqiang Li:** Writing – original draft, Resources, Project administration, Investigation. **Jun Deng:** Writing – review & editing, Investigation.

Declaration of Competing Interest

The authors declare that they have no known competing financial interests or personal relationships that could have appeared to influence the work reported in this paper.

Data availability

Data will be made available on request.

Acknowledgements

This study was supported by two grants to Keke Sun (the National Natural Science Foundation of China: No. 42003024; Open Research Project from the State Key Laboratory for Mineral Deposits Research, Nanjing University: No. 2020-LAMD-K11). The Fundamental Research Funds for the Central Universities (No. 14380165, 14380126, 14380141, to WLi). The authors wish to thank Xiaolin Cui, Rong Xu, and Hanyu Cheng and the staff of Yunnan Tin Group for their valuable help during field-works. We thank Editor Claudia Romano for efficient and rigorous editorial handling, and Huan Li and another anonymous reviewer for their constructive comments and criticism that lead to significant improvement of the manuscript.

Appendix A. Supplementary data

Supplementary data to this article can be found online at https://doi.org/10.1016/j.chemgeo.2023.121843.

References

Audétat, A., 2019. The Metal Content of Magmatic-Hydrothermal Fluids and its Relationship to Mineralization potential. Econ. Geol. 114, 1033–1056.
Badullovich, N., Moynier, F., Creech, J., Teng, F.Z., Sossi, P.A., 2017. Tin isotopic fractionation during igneous differentiation and Earth's mantle composition. Geochem. Persp. Let. 5, 24–28.
Brügmann, G., Berger, D., Pernicka, E., 2017. Determination of the Tin Stable Isotopic Composition in Tin-bearing Metals and Minerals by MC-ICP-MS. Geostand. Geoanal. Res. 41, 437–448.
Caricchi, L., Blundy, J., 2015. Experimental petrology of monotonous intermediate magmas. Geol. Soc. Lond. Spec. Publ. 422, 105–130.
Chen, B., Huang, C., Zhao, H., 2020. Lithium and Nd isotopic constraints on the origin of Li-poor pegmatite with implications for Li mineralization. Chem. Geol. 551, 119769.
Cheng, Y., Mao, J., 2010. Age and geochemistry of granites in Gejiu area, Yunnan province, SW China: Constraints on their petrogenesis and tectonic setting. Lithos 120, 258–276.
Cheng, Y., Mao, J., Rusk, B., Yang, Z., 2012. Geology and genesis of Kafang Cu–Sn deposit, Gejiu district, SW China. Ore Geol. Rev. 48, 180–196.
Cheng, Y., Mao, J., Chang, Z., Pirajno, F., 2013a. The origin of the world class tin-polymetallic deposits in the Gejiu district, SW China: Constraints from metal zoning characteristics and 40Ar–39Ar geochronology. Ore Geol. Rev. 53, 50–62.
Cheng, Y., Mao, J., Spandler, C., 2013b. Petrogenesis and geodynamic implications of the Gejiu igneous complex in the western Cathaysia block, South China. Lithos 175-176, 213–229.
Creech, J.B., Moynier, F., Badullovich, N., 2017. Tin stable isotope analysis of geological materials by double-spike MC-ICP-MS. Chem. Geol. 457, 61–67.
Deng, G., Jiang, D., Zhang, R., Huang, J., Zhang, X., Huang, F., 2022. Barium isotopes reveal the role of deep magmatic fluids in magmatic-hydrothermal evolution and tin enrichment in granites. Earth Planet. Sci. Lett. 594, 117724.
Durasova, N.A., Ryabchikov, I.D., Barsukov, V.L., 1986. The redox potential and the behavior of tin in magmatic systems. Int. Geol. Rev. 28, 305–311.
Fan, J.-J., Wang, Q., Ma, L., Li, J., Zhang, X.-Z., Zhang, L., Wang, Z.-L., 2022. Extreme Mo isotope variations recorded in high-SiO_2 granites: Insights into magmatic differentiation and melt–fluid interaction. Geochim. Cosmochim. Acta 334, 241–258.
Farges, F., Linnen, R.L., Brown Jr., G.E., 2006. Redox and speciation of tin in hydrous silicate glasses: a comparison with Nb, Ta, Mo and W. Can. Mineral. 44, 795–810.
Harlaux, M., Kouzmanov, K., Gialli, S., Clark, A.H., Laurent, O., Corthay, G., Prado Flores, E., Dini, A., Chauvet, A., Ulianov, A., Chiaradia, M., Menzies, A., Villón Durand, G., Kalinaj, M., Fontboté, L., 2021. The upper Oligocene San Rafael intrusive complex (Eastern Cordillera, Southeast Peru), host of the largest-known high-grade tin deposit. Lithos 400-401, 106409.
Haustein, M., Gillis, C., Pernicka, E., 2010. Tin isotopy–a new method for solving old questions. Archaeometry 52, 816–832.
He, Y., Wu, H., Ke, S., Liu, S.-A., Wang, Q., 2017. Iron isotopic compositions of adakitic and non-adakitic granitic magmas: Magma compositional control and subtle residual garnet effect. Geochim. Cosmochim. Acta 203, 89–102.
Holtz, F., Tamic, N., Behrens, H., 2001. Maximum and minimum water contents of granitic melts generated in the crust: a reevaluation and implications. Lithos 56, 1–14.
Icenhower, J.P., London, D., 1997. Partitioning of fluorine and chlorine between biotite and granitic melt: experimental calibration at 200 MPa H2O. Contrib. to Mineral. Petrol. 127, 17–29.
Ishihara, S., 1977. The magnetite-series and ilmenite-series granitic rocks. Mining geology 27, 293–305.
Jahn, B.M., Wu, F., Capdevila, R., Martineau, F., Zhao, Z., Wang, Y., 2001. Highly evolved juvenile granites with tetrad REE patterns: the Woduhe and Baerzhe granites from the Great Xing'an Mountains in NE China. Lithos 59, 171–198.
Lehmann, B., 1982. Metallogeny of tin: magmatic differentiation versus geochemical heritage. Econ. Geol. 77, 50–59.
Lehmann, B., 2021. Formation of tin ore deposits: a reassessment. Lithos 402-403, 105756.
Lehmann, B., Mahawat, C., 1989. Metallogeny of tin in Central Thailand: a genetic concept. Geology 17, 426–429.
Li, X., Zhang, C., 2022. Machine Learning Thermobarometry for Biotite-Bearing Magmas. Journal of Geophysical Research: Solid. Earth 127 (e2022JB024137).
Linnen, R.L., Pichavant, M., Holtz, F., 1996. The combined effects of fO_2 and melt composition on SnO_2 solubility and tin diffusivity in haplogranitic melts. Geochim. Cosmochim. Acta 60, 4965–4976.
Liu, P., Mao, J., Lehmann, B., Weyer, S., Horn, I., Mathur, R., Wang, F., Zhou, Z., 2021. Tin isotopes via fs-LA-MC-ICP-MS analysis record complex fluid evolution in single cassiterite crystals. Am. Mineral. 106, 1980–1986.
Loucks, R.R., Fiorentini, M.L., Henríquez, G.J., 2020. New Magmatic Oxybarometer using Trace elements in Zircon. J. Petrol. 61, 1–30.
Mao, J., Cheng, Y., Chen, M., Franco, P., 2013. Major types and time–space distribution of Mesozoic ore deposits in South China and their geodynamic settings. Miner. Depos. 48, 267–294.
Nash, W.P., Crecraft, H.R., 1985. Partition coefficients for trace elements in silicic magmas. Geochim. Cosmochim. Acta 49, 2309–2322.
Rasmussen, K.L., Mortensen, J.K., 2013. Magmatic petrogenesis and the evolution of (F:Cl:OH) fluid composition in barren and tungsten skarn-associated plutons using apatite and biotite compositions: Case studies from the northern Canadian Cordillera. Ore Geol. Rev. 50, 118–142.
Roskosz, M., Amet, Q., Fitoussi, C., Dauphas, N., Bourdon, B., Tissandier, L., Hu, M.Y., Said, A., Alatas, A., Alp, E.E., 2020. Redox and structural controls on tin isotopic fractionations among magmas. Geochim. Cosmochim. Acta 268, 42–55.
Rudnick, R.L., Gao, S., 2003. Composition of the Continental Crust. In: Holland, H.D., Turekian, K.K. (Eds.), Treatise on Geochemistry. Pergamon, Oxford, pp. 1–64.
She, J.-X., Wang, T., Liang, H., Muhtar, M.N., Li, W., Liu, X., 2020. Sn isotope fractionation during volatilization of Sn(IV) chloride: Laboratory experiments and quantum mechanical calculations. Geochim. Cosmochim. Acta 269, 184–202.
She, J.-X., Kubik, E., Li, W., Moynier, F., 2023a. Stable Sn isotope signatures of Mid-ocean ridge basalts. Chem. Geol. 622, 121347.
She, J.-X., Li, W., An, S., Cai, Y., 2023b. High-precision double-spike Sn isotope analysis of geological materials by MC-ICP-MS. J. Anal. At. Spectrom 38, 142–155.
Shimizu, K., Itai, T., Kusakabe, M., 2006. Ion Chromatographic Determination of Fluorine and Chlorine in Silicate Rocks following Alkaline Fusion. Geostand. Geoanal. Res. 30, 121–129.
Simons, B., Andersen, J.C.Ø., Shail, R.K., Jenner, F.E., 2017. Fractionation of Li, be, Ga, Nb, Ta, in, Sn, Sb, W and Bi in the peraluminous early Permian Variscan granites of the Cornubian Batholith: Precursor processes to magmatic-hydrothermal mineralisation. Lithos 278-281, 491–512.
Spera, F.J., Bohrson, W.A., Till, C.B., Ghiorso, M.S., 2007. Partitioning of trace elements among coexisting crystals, melt, and supercritical fluid during isobaric crystallization and melting. Am. Mineral. 92, 1881–1898.
Stepanov, A., Mavrogenes, A., Meffre, S., Davidson, P., 2014. The key role of mica during igneous concentration of tantalum. Contrib. Mineral. Petrol. 167, 1009.
Sun, S.-S., McDonough, W.F.J.G.S., 1989. Chemical and isotopic systematics of oceanic basalts: implications for mantle composition and processes. Geo. Soc. Lond. Spec. Publ. 42, 313–345.
Sun, H., Gao, Y., Xiao, Y., Gu, H.-O., Casey, J.F., 2016. Lithium isotope fractionation during incongruent melting: Constraints from post-collisional leucogranite and residual enclaves from Bengbu Uplift, China. Chem. Geol. 439, 71–82.
Sun, K., Chen, B., Deng, J., 2019. Biotite in highly evolved granites from the Shimensi W–Cu–Mo polymetallic ore deposit, China: Insights into magma source and evolution. Lithos 350-351, 105245.

Sun, K.-K., Deng, J., Wang, Q.-F., Chen, B., Xu, R., Ma, Z.-F., 2023. Formation of Sn-rich granitic magma: a case study of the highly evolved Kafang granite in the Gejiu tin polymetallic ore district, South China. Miner. Depos. 58, 359–378.
Telus, M., Dauphas, N., Moynier, F., Tissot, F.L.H., Teng, F.-Z., Nabelek, P.I., Craddock, P. R., Groat, L.A., 2012. Iron, zinc, magnesium and uranium isotopic fractionation during continental crust differentiation: the tale from migmatites, granitoids, and pegmatites. Geochim. Cosmochim. Acta 97, 247–265.
Wang, X., Fitoussi, C., Bourdon, B., Amet, Q., 2017. A new method of Sn purification and isotopic determination with a double-spike technique for geological and cosmochemical samples. J. Anal. At. Spectrom 32, 1009–1019.
Wang, X., Amet, Q., Fitoussi, C., Bourdon, B., 2018. Tin isotope fractionation during magmatic processes and the isotope composition of the bulk silicate Earth. Geochim. Cosmochim. Acta 228, 320–335.
Wang, D., Mathur, R., Powell, W., Godfrey, L., Zheng, Y., 2019. Experimental evidence for fractionation of tin chlorides by redox and vapor mechanisms. Geochim. Cosmochim. Acta 250, 209–218.
Wang, T., She, J.-X., Yin, K., Wang, K., Zhang, Y., Lu, X., Liu, X., Li, W., 2021. Sn(II) chloride speciation and equilibrium Sn isotope fractionation under hydrothermal conditions: a first principles study. Geochim. Cosmochim. Acta 300, 25–43.
Wang, Z.-Y., Luo, Z.-Y., Zhang, L., Liu, J.-J., Li, J., 2022. Sn Isotopic Values in ten Geological Reference Materials by Double-Spike MC-ICP-MS. Geostand. Geoanal. Res. 46, 547–561.
Webster, J.D., Holloway, J.R., 1990. Partitioning of F and Cl between magmatic hydrothermal fluids and highly evolved granitic magmas. In: Stein, H.J., Hannah, J. L. (Eds.), Ore-Bearing Granite Systems; Petrogenesis and Mineralizing Processes. Geological Society of America, pp. 21–34.
Webster, J.D., Tappen, C.M., Mandeville, C.W., 2009. Partitioning behavior of chlorine and fluorine in the system apatite–melt–fluid. II: Felsic silicate systems at 200MPa. Geochim. Cosmochim. Acta 73, 559–581.
Wu, J., Li, H., Mathur, R., Bouvier, A., Powell, W., Yonezu, K., Zhu, D., 2023. Compositional Variation and Sn Isotope Fractionation of Cassiterite during Magmatic-Hydrothermal Processes. Earth. Planet. Sci. Lett., p. 613
Xu, R., Romer, R.L., Glodny, J., 2021. External fluids cause alteration and metal redistribution in the granite-hosted Tangziwa Sn Cu deposit, Gejiu district, China. Lithos 382-383, 105937.
Xu, R., Romer, R.L., Glodny, J., 2022a. Metal mobilization and precipitation in a Sn-W skarn system, Gejiu Sn district, China. Lithos 414-415, 106621.
Xu, R., Romer, R.L., Kroner, U., Deng, J., 2022b. Tectonic control on the spatial distribution of Sn mineralization in the Gejiu Sn district, China. Ore Geol. Rev. 148, 105004.
Yamazaki, E., Nakai, S., Rsquo, Ich, Yokoyama, T., Ishihara, S., Tang, H., 2013. Tin isotope analysis of cassiterites from Southeastern and Eastern Asia. Geochem. J. 47, 21–35.
Yamazaki, E., Nakai, S., Sahoo, Y., Yokoyama, T., Mifune, H., Saito, T., Chen, J., Takagi, N., Hokanishi, N., Yasuda, A., 2014. Feasibility studies of Sn isotope composition for provenancing ancient bronzes. J. Archaeol. Sci. 52, 458–467.
Yao, J., Mathur, R., Powell, W., Lehmann, B., Tornos, F., Wilson, M., Ruiz, J., 2018. Sn-isotope fractionation as a record of hydrothermal redox reactions. Am. Mineral. 103, 1591–1598.
Zajacz, Z., Halter, W.E., Pettke, T., Guillong, M., 2008. Determination of fluid/melt partition coefficients by LA-ICP-MS analysis of co-existing fluid and silicate melt inclusions: Controls on element partitioning. Geochim. Cosmochim. Acta 72, 2169–2197.
Zhang, D., Bao, Z., Liu, P., Brügmann, G., Yang, W., Chen, K., Liang, P., Yuan, H., 2023. A high-temperature sintered cassiterite reference material for in situ determination of Sn isotope ratios. J. Anal. At. Spectrom 38, 204–211.
Zhao, P., Chu, X., Williams-Jones, A.E., Mao, J., Yuan, S., 2022a. The role of phyllosilicate partial melting in segregating tungsten and tin deposits in W-Sn metallogenic provinces. Geology 50, 121–125.
Zhao, P., Zajacz, Z., Tsay, A., Yuan, S., 2022b. Magmatic-hydrothermal tin deposits form in response to efficient tin extraction upon magma degassing. Geochim. Cosmochim. Acta 316, 331–346.
Zhou, Z.-H., Mao, J.-W., Zhao, J.-Q., Gao, X., Weyer, S., Horn, I., Holtz, F., Sossi, P.A., Wang, D.-C., 2022. Tin isotopes as geochemical tracers of ore-forming processes with Sn mineralization. Am. Mineral. 107, 2111–2127.
Zhu, C., Sverjensky, D.A., 1991. Partitioning of F-Cl-OH between minerals and hydrothermal fluids. Geochim. Cosmochim. Acta 55, 1837–1858.